Andean Geology 49 (3): 327-344. September, 2022
doi: 10.5027/andgeoV49n3-3340

Andean Geology
www.andeangeology.cl

The Iglesia basin (San Juan, Argentina), seismic interpretation, geometry basin, and implications for geothermal systems

***Marcos Podesta[1], Gustavo Ortiz[1, 2], Paola Orozco[1], [†]Patricia Alvarado[1, 2], Facundo Fuentes[3]**

[1] *Centro de Investigaciones de la Geósfera y la Biósfera (CIGEOBIO), Facultad de Ciencias Exactas, Físicas y Naturales, Universidad Nacional de San Juan-Consejo Nacional de Investigaciones Científicas y Técnicas (CONICET), Meglioli 1160 S (5406) Rivadavia, San Juan, Argentina.*
marcospodesta@unsj-cuim.edu.ar; gfortiz@unsj-cuim.edu.ar; paola.orozco@unsj-cuim.edu.ar; alvarado@unsj.edu.ar

[2] *Departamento de Geofísica y Astronomía, Facultad de Ciencias Exactas, Físicas y Naturales, Universidad Nacional de San Juan, Meglioli 1160 S (5406) Rivadavia, San Juan, Argentina.*

[3] *YPF S.A. Macacha Güemes 515, C1107 CABA, Argentina.*
facundo.fuentes@ypf.com

**Corresponding author: marcospodesta@unsj-cuim.edu.ar*

ABSTRACT. The Iglesia basin, in the San Juan Province, is the northern part of a Cenozoic piggy-back basin (the Iglesia-Calingasta-Uspallata basin), located above of the active flat-slab subduction zone of western Argentina. This basin is located between two mountain ranges, the Cordillera Frontal to the west and the Precordillera to the east, affected by thin and thick skinned tectonics, respectively. It is elongated in a north-south direction (70 km) and has a maximum width of 35 km. We have analyzed 17 seismic reflection lines corresponding to more than 500 km of interpreted sections. A strong reflection at 0.5-2 s is interpreted as indicative of shales and sandstones in the upper part of the Agua Negra Formation (Carboniferous); this represents a seismic basement for the Iglesia basin clearly separating stratified (shallower) from chaotic (deeper) reflectors. Several high angle faults have been recognized in the interpreted seismic lines affecting the Neogene fill and even the basement; some of them correlate with structures observed at the surface such us El Tigre Fault System. A 3D model shows the seismic top of basement smoothly deepening down to 3,650 m beneath the Pismanta area. The basement continues upward to the east with a steeper slope clearly defining an asymmetrical shape for the basin. Moreover, there are three depocenters of similar maximum depths around the geothermal hot spring of the Pismanta center. Some of the interpreted faults may be helping in the outflow process of meteoric water heated by a normal geothermal gradient. Considering earthquake data framework, our observations correlate with transpressive deformation likely associated with El Tigre Fault System, which affects Neogene and Pleistocene strata of the Iglesia Group.

Keywords: Frontal Cordillera, Precordillera, Piggyback basin, Pismanta geothermal area, Seismic interpretation.

RESUMEN. La cuenca de Iglesia (San Juan, Argentina), interpretación sísmica, geometría e implicaciones para los sistemas geotérmicos. La cuenca del valle de Iglesia corresponde a la parte norte de la cuenca de Iglesia-Calingasta-Uspallata, ubicada sobre la zona de subducción plana en el oeste de Argentina. Esta cuenca se localiza entre la Cordillera Frontal (oeste) y la Precordillera (este), con una longitud de aproximadamente 70 km en dirección norte-sur y 35 km de ancho máximo en dirección este-oeste. Con el objeto de caracterizar la cuenca en profundidad, se analizaron 17 líneas de reflexión sísmica correspondientes a más de 500 km de secciones interpretadas. Un marcado reflector sísmico identificado alrededor de 0,5 a 2 s, es interpretado como el techo de la Formación Agua Negra de edad carbonífera (lutitas y areniscas); este es interpretado como un basamento sísmico para la cuenca del valle de Iglesia y separa los reflectores estratificados (menos profundos) de los caóticos (más profundos). Estructuralmente, se han reconocido varias fallas de alto ángulo en los perfiles sísmicos, estas afectan al relleno neógeno de la cuenca y el basamento. Solo algunas de estas fallas se correlacionan con estructuras observadas en la superficie, como el Sistema de Falla El Tigre. Un modelo 3D muestra el basamento sísmico profundizándose suavemente hasta 3.650 m directamente debajo del área donde se ubica la fuente termal de Pismanta, otros dos depocentros de profundidades similares están presentes en esta área. Desde el centro de la cuenca el basamento presenta una pendiente más pronunciada, hacia el este que hacia el oeste, definiendo así una forma asimétrica para la cuenca. Algunas de las fallas reconocidas en las secciones sísmicas pueden

estar contribuyendo al proceso de ascenso del agua meteórica que aumentó su temperatura por la acción de un gradiente geotérmico normal. Los mecanismos focales de los terremotos que han afectado el área y nuestras observaciones son compatibles con un evento de deformación transpresiva probablemente asociado al Sistema de Falla El Tigre y que afecta los estratos del Neógeno y Pleistoceno del Grupo Iglesia.

Palabras clave: Cordillera Frontal, Precordillera, Cuenca, Fuente geotermal, Pismanta; Interpretación sísmica.

1. Introduction

The Iglesia basin is located 300 km east of the pacific trench related to the interaction of the Nazca and South American plates, with a convergence rate of about 64 mm/yr (Vigny *et al*., 2009), and about 110 km above the subducted slab (Ammirati *et al*., 2016). The basin is the northern portion of the ~150 km long Iglesia-Calingasta-Uspallata basin between the Precordillera in the east, with an elevation of about 2,500 m a.s.l. and the Cordillera Frontal in the west, with an elevation of about 5,000 m a.s.l. (Figs. 1 and 2). The oceanic Nazca plate slab in this segment of the Andes has a nearly horizontal position, something only observed in 10% of the convergent margins on Earth. Not many of these flat-slab regions show mountainous continental chains with a wide intervening basin (like the Iglesia basin) in their backarc regions (Gutscher *et al*., 2000) (Fig. 1). Shallow subduction processes at the latitude of the study area (30° S) seem to have started at *ca.* 10-5 Ma according to magmatic, sedimentary and thermochronological studies (Jordan *et al.,* 1993; Kay *et al.,* 2005; Fosdick *et al*., 2015; Mackaman-Lofland *et al*., 2020).

Previous studies in this northern area of the Iglesia-Calingasta-Uspallata basin proposed that it includes a Neogene sequence up to 3.5 km thick, and it is interpreted as a piggyback basin that was developed during the eastward propagation of deformation within the Precordilleran thrusts (Beer *et al*., 1990; Jordan *et al*., 1993). Former interpretations using seismic reflection data showed the Iglesia basin highly affected by a zone of deformation in its eastern part (Álvarez-Marrón *et al*., 2006), with steep reverse faults and folding of the sedimentary fill near the locality of Rodeo (~30.2° S; ~69.0° W). This area also contains the presence of the Pismanta mesothermal (45 °C) water spring center whose temperature is lower than that of the geothermal centers in the high Cordillera of about 75 °C (Sussini *et al*., 1948) (Fig. 1). This has gained importance in recent years due to the possibility of geothermal energy generation and socioeconomy-tourism development. Because of the flat slab subduction, there is no active volcanism in the Frontal Cordillera and Precordillera in the San Juan area (Kay *et al*., 1991). The association of geothermal areas in the Precordillera with a volcanic origin is thus not expected; however relatively higher temperature centers are present in the high Cordillera, such as Despoblados water springs linked to a magmatic heating source (Sussini *et al*., 1948); those areas, are located in remote low populated areas in the northwest of San Juan. In the Iglesia Valley there are also other thermal spring sources such as Centenario, Poblete at about 30 km distance from Pismanta, which are considered as part of the same geothermal system in this study (Figs. 1 and 2).

This work presents a characterization of the Iglesia Valley basin, generating a Move model (MVE: Midland Valley and Petroleum Experts. https://www.mve.com/) with the main goal to delimitate its seismic basement as well as other geological structures around the hydrothermal system of Pismanta with available information. The shape of the basin (with its points of maximum depth) will be correlated with the location of the geothermal sources. We interpreted about 500 km form a set of seventeen seismic reflection lines acquired by YPF S.A. in the 90's. The work involved the 2D analysis of each seismic line in order to identify major faults, folds, the basement shape, the horizontal continuity of geological units as well as their correlation in contiguous 2D lines and in the surface.

2. Geological framework

The region of study comprises two different tectono-stratigraphic terranes, Chilenia in the west and Cuyania to the east (Fig. 1), being separated by a dissected belt of ophiolitic rocks. The Chilenia terrane is composed of high grade metamorphic rocks exposed to the west of the ophiolitic belt (Ramos *et al*., 2010). According to Ramos (2004) the Cuyania terrane, in the Western Sierras Pampeanas and the Precordillera, exhibits Grenville rocks and

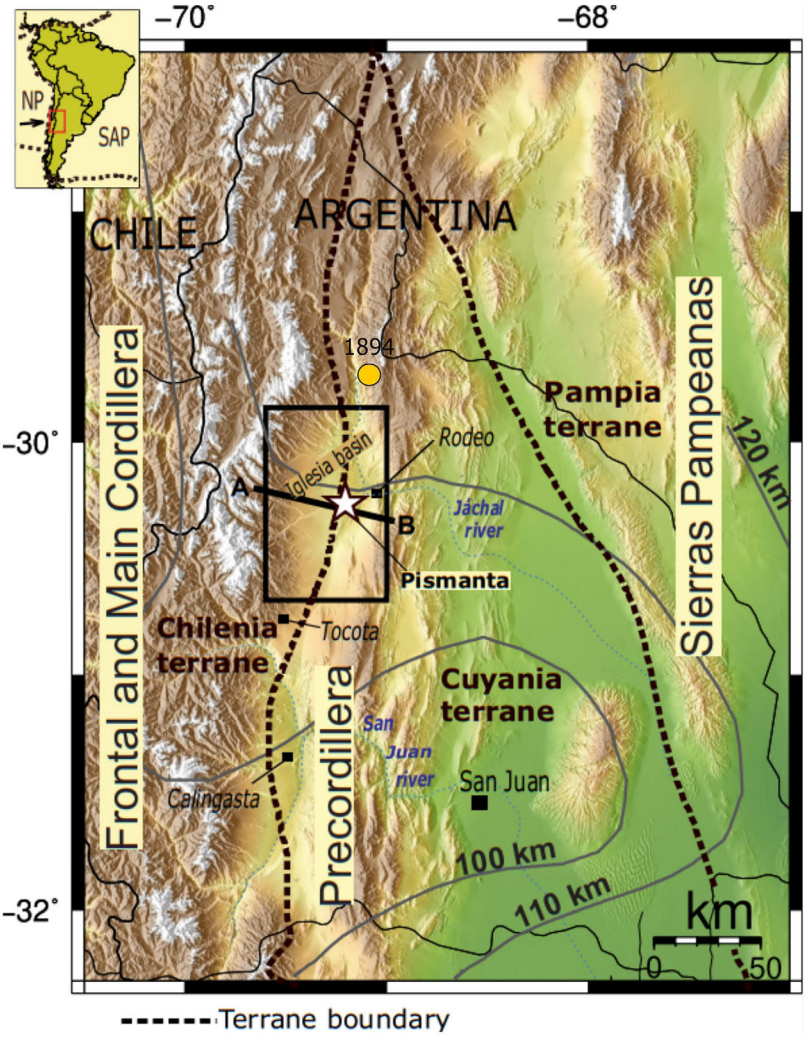

FIG. 1. Study region (rectangle) showing morphostructural units and terranes (Ramos, 1995, 1999; Astini *et al*., 1996), the 1894 (M>7) earthquake epicenter (yellow dot), and the cross section over the Pismanta geothermal system (A-B), which is shown in figure 2. Also shown are the depth contours, in km, of the Nazca Plate (NP) beneath the South American Plate (SAP) according to Anderson *et al.* (2007) and localities (black squares) mentioned in the text. The arrow in the inset represents the GPS relative convergence velocity between the NP and SAP according to Vigny *et al.* (2009).

Laurentian carbonate platform rocks of Cambrian-Ordovician age (Astini *et al*., 1996) (Fig. 1). Ramos (1984) suggests that the Chilenia and Cuyania terranes were both part of Laurentia and were later accreted to the western margin of Gondwana during Ordovician and Devonian time. The presence of about ~300 km igneous calcoalkaline rocks of Eopaleozoic ages has been related to the approach and collision of the Chilenia terrane, although its genesis and the geotectonic framework in which they have been originated are not fully understood (*e.g*., Pérez, 2015).

The Iglesia basin is located in the northwestern part of the San Juan province, between 30° S and 31° S and between 69° W and 69°30’ W. From the Miocene, the compressive tectonics controls the structure of this region due to the flat slab subduction between the Nazca Plate and the South American Plate between 28° S and 32° S (Fig. 2) (Barazangi and Isacks, 1976; Cahill and Isacks, 1992; Anderson *et al*., 2007; Ammirati *et al*., 2015, 2016). To the west, the tectonic of the Frontal Cordillera is dominated by mechanical basement-

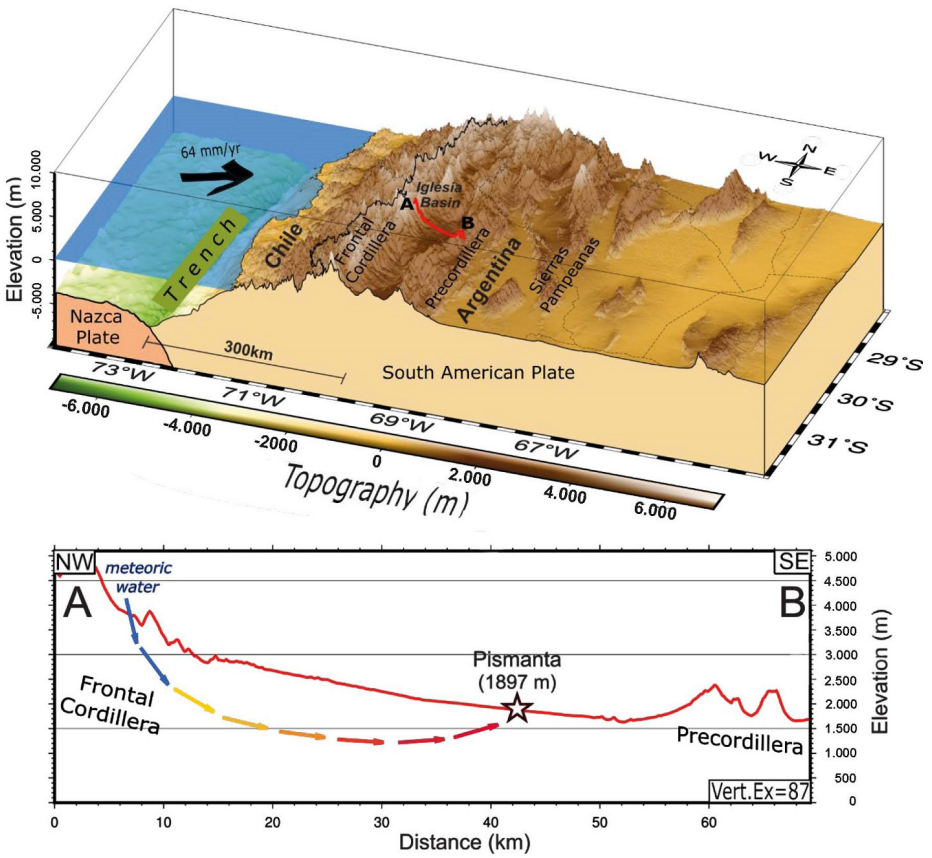

FIG. 2. 3D view (upper panel) and elevation profile A-B (lower panel) across the Pismanta geothermal system (see Fig. 1 for location). The Iglesia Valley elevations are between 1,600 and 3,500 m a.s.l. The black arrow in the upper panel denotes the relative plate convergence velocity and direction according to Vigny *et al.* (2009). Blue, yellow and red arrows in the lower panel represent the schematic meteoric water track.

involved uplifts that exhume predominantly Upper Paleozoic-Triassic rhyolites and granitic intrusions, in addition Devonian-Carboniferous metamorphic and sedimentary rocks are also exposed (Heredia *et al*., 2002; Kleiman and Japas, 2009; Vallecillo *et al*., 2010; Rocher and Vallecillo, 2014). To the east, the Western Precordillera thin skinned fold-thrust belt bounds the basin; this fold-thrust belt extends to the foreland accommodating the majority of the retroarc shortening (>100 km) and involves Paleozoic-lower Mesozoic sedimentary rocks and Cenozoic deposits (Allmendinger *et al*., 1990; Von Gosen, 1992; Cristallini and Ramos, 2000).

Sedimentological studies carried out by Wetten (1975), Beer *et al*. (1990) and Ré *et al*. (2003) have described the Neogene to Pleistocene fill of the Iglesia basin, which is composed of sedimentary sequences of continental origin. The Iglesia Group involves the Pliocene Las Flores Formation and Miocene Lomas del Campanario Formation. (Fig. 3). According to Allmendinger *et al*. (1990), this sedimentation coexisted with the thrusts of the Precordillera whose main structures dip westward; thus, this basin constitutes a piggyback basin, which is being passively transported eastward on the activity of the Frontal Cordillera. The Carboniferous shale, sandstone and conglomerate of the Agua Negra Formation are observed on the west side of the valley, as part of the Frontal Cordillera, but not in the Precordillera on its eastern edge (Figs. 2 and 3); Yerba Loca Formation (composed of shales, sandstones and Ordovician basalts) is also observed on the west side of the valley (Fig. 3). We assume this may correspond to the basement of the Iglesia basin. The volcanic

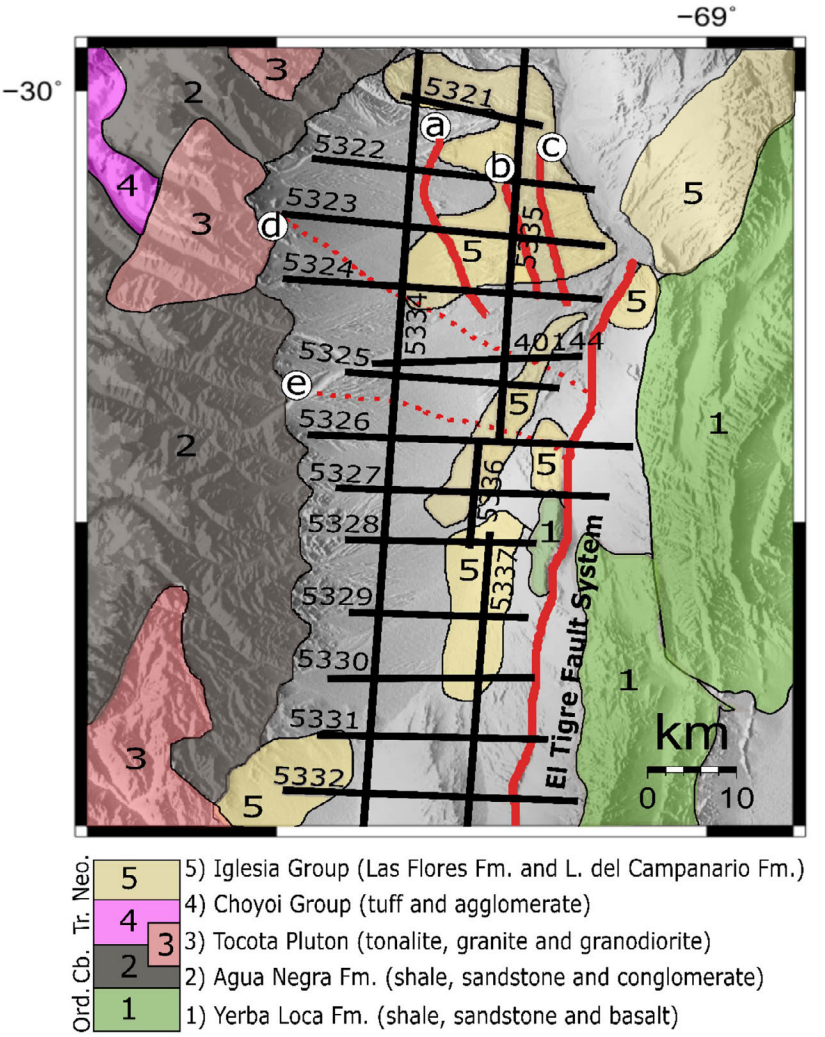

FIG. 3. Location of seismic reflection lines (black lines with their corresponding identification numbers) on the geological map of Cardó *et al.* (2005). El Tigre Fault System, in solid red lines, according to Perucca and Vargas (2014); **a**, **b** and **c** are faults observed at the surface with continuity in depth as shown in the interpreted seismic lines. Red dashed lines (**d**) and (**e**) correspond to inferred faults at depth from this work. **Ord.:** Ordovician, **Cb.:** Carboniferous, **Tr.:** Triassic, **Neo.:** Neogene.

Permo-Triassic rocks of Choyoi Group also outcrop to the west of the valley (Frontal Cordillera) but not in its eastern margin (Precordillera). Wetten (1975) described the Pliocene Las Flores Formation as an upper member composed of conglomerates and a lower member made up of clays, limolites and fine sandstones. The Miocene Lomas del Campanario Formation is composed of two members, an agglomerate member consisting of pyroclastic material, andesites, dacites and andesitic tuffs and a conglomerate member with a high content of volcanoclastic rocks (Wetten, 1975). A Miocene to Pliocene pyroclastic sequence associated with lava flows and subvolcanic rocks is exposed along the Iglesia Valley Basin (Poma *et al*., 2017). In This sedimentary filling of the basin is consistent with predominantly Neogene deposits (Beer *et al*., 1990; Ré *et al*., 2003) originally deposited in a former Oligocene foreland basin (Jordan *et al*., 2001).

Structurally, the main feature in the western sector of the Precordillera is the El Tigre fault extending for more than 100 km between the Jáchal and San Juan rivers (Figs. 1 and 3). Dominant oblique slip movement with a dextral component has been

suggested for this regional fault (Bastías, 1986; Wetten, 1975; Siame *et al*., 1996, 1997; Fazzito, 2011; Ruskin and Jordan, 2007). Pérez and Costa (2006), Perucca and Vargas (2014) and Rivas *et al*. (2019) have proposed that the non-instrumentally recorded 1894 (Fig. 1) earthquake of magnitude M>7 (Richter scale) may have occurred in the northern continuation of the El Tigre fault system. Some exposed segments of this fault show an average strike of N10°±6° and an almost vertical dip (Costa *et al*., 2000); it affects six levels of alluvial fans with ages varying between 700,000 years for the oldest levels and 21,000 years for the most recent surfaces of the current level (Siame *et al*., 1997).

3. Hot springs

Several hot springs are located in the east-central part of the Iglesia Valley near the town of Pismanta (Fig. 1) and other neighboring areas such as Centenario, Carrizalito, Rosales, Horcones, Arnobio, Poblete and La Salud (Fig. 4). We have

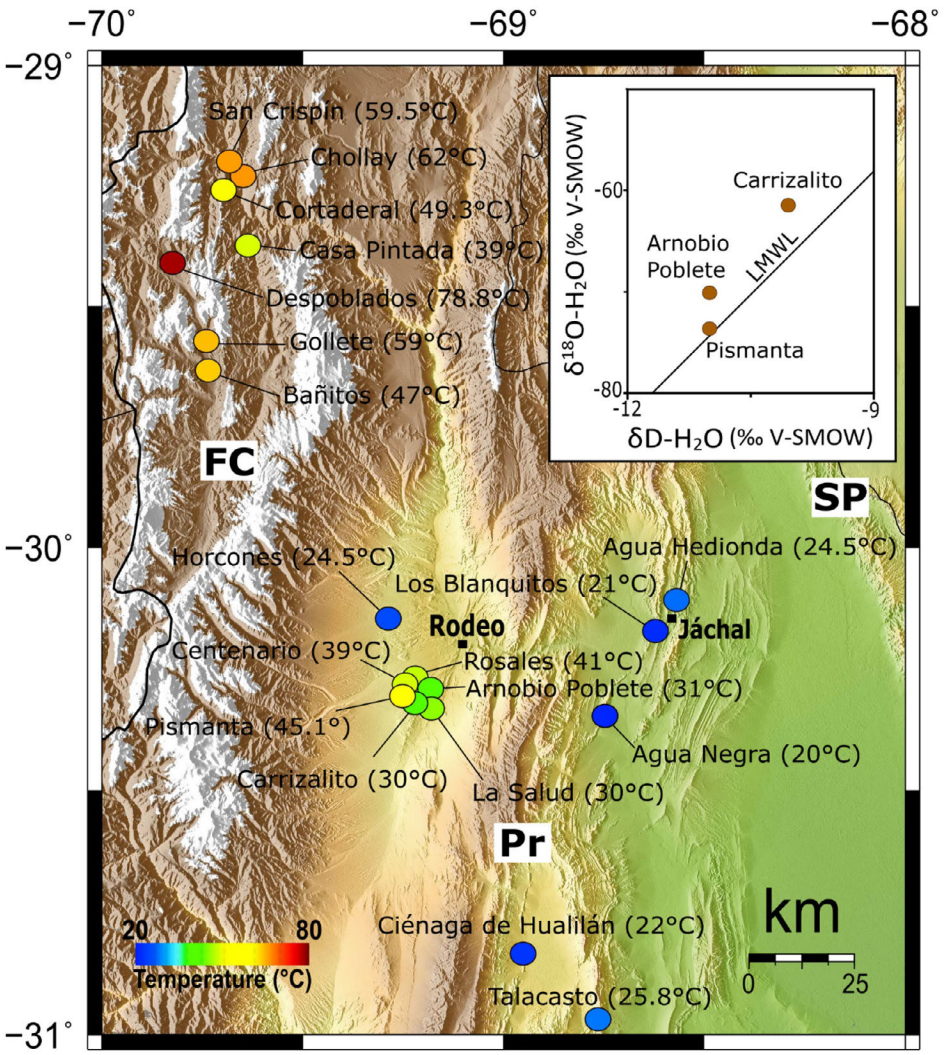

FIG. 4. Locations of hot springs with their temperatures (Sussini *et al*., 1948) showing variations between higher temperature values in the Frontal Cordillera (**FC**) to lower temperature values in the Precordillera (**Pr**); the Iglesia Valley water springs water exhibit values in between. Isotope data from Esin (1982) are shown in the inset for thermal springs Pismanta, Carrizalito and Arnobio Poblete. The local meteoric water line (**LMWL**) is from Hoke *et al*. (2013).

used basic geochemical data of fluids in this sector by Sussini *et al*. (1948) to infer features from deep fluid reservoirs and their possible association with faults in this area. Measurements of the water source temperature at surface indicate relatively low enthalpy hypothermal springs (Muffler, 1979; Hochstein, 1988; Benderitter and Corny, 1990; Haenel *et al*., 1988), with temperatures <45 °C. At a regional scale, higher temperatures (~70 °C) hot springs are observed in the high Andes westward (Sussini *et al*., 1948; Barcelona *et al*., 2014); in contrast lower temperatures (~20 °C) hot springs characterize the eastern Precordillera to the east (Fig. 4). One possible explanation for the relatively higher temperature water sources outflowing at the surface near Pismanta, in the central eastern part of the Iglesia Valley, would be that the high elevation regions in the west (>5,000 m a.s.l.) allow the infiltration of rain and snow meteoric water into the system. Then, differences in the slope (Fig. 2) favor the infiltrated water motion from west to east while it heats up by a normal geothermal gradient. The water hosted in deep reservoirs may be reaching the fault systems in the east (western-central Precordillera). Thus, the fault system plays a role controlling the hydrothermal system. Another hypothesis suggests that recent isolated magmatism would contribute as a source in the heating of infiltrated meteoric water in tectonic environments associated with horizontal subduction; an example has been described in Despoblados area in the high Andes as a geothermal system (see location in Fig. 4) by Barcelona *et al.* (2014, 2019a, b).

Compositionally, the Pismanta waters are classified as sodium sulfates ($SO_4^{2-}Na^+$) (Sussini *et al*., 1948). Ca-Na, Ca-K, Na-K and Silica geothermometers (Tonani, 1980; Fournier, 1983) were used to obtain reservoir temperatures; they yielded values of 155 °C, 69 °C, 49 °C and 91 °C, respectively; two of these geothermometer values (Ca-K and Silica) were also reported in the inventory by Pesce and Miranda (2003). Assuming these values of 69 °C and 91 °C, respectively, and a normal geothermal gradient of 28 °C/km (obtained from the Ansilta oil exploration well in the Calingasta Valley), it is possible to estimate reservoir depths of 945 m and 1,800 m. However, it is worth to note that Sussini *et al.* (1948) have even observed a greater variation of more than 105 °C over the four geothermometers. Thus, we suggest the presence of two reservoirs located at depths of less than 1 km and more than 2 km, respectively. Data on stable isotope composition consisting in $^{18}O/^{16}O$ and $^{2}H/^{1}H$ ratios from Pesce and Miranda (2003) clearly show a meteoric origin for the water in three samples from thermal springs near Pismanta (Fig. 4). The Carrizalito and Arnobio Poblete springs show a significant ^{18}O-depletion likely due to isotopic exchange between liquid water and CO_2, a process that typically affects CO_2-rich bubbling pools (Epstein and Mayeda, 1953; Pauwels *et al*., 1997) and HCO_3 hydrothermally enriched waters (Peiffer *et al*., 2014) (Fig. 4).

4. Methodology

A 2D view was used line by line to recognize each reflector and faults. Furthermore, a 3D view was used at the end in order to identify the lateral continuity of the reflectors previously recognized in each seismic line individually and the continuity of faults as well. In this work we have analyzed information from more than 500 linear km of seismic reflection data from the industry, located in the Iglesia Valley (Fig. 3). This work was done on the MOVE™ platform with an academic license (https://www.mve.com/). These lines were acquired using an energy detonating cord as a seismic source, with a fold of 2,400% (line 40144 has a fold of 1,200%). The length of the lines varies from 25 km to 100 km for the longest north-south line (5334). The processing of the seismic lines followed the standard sequence of pre-stacking, stacking and post-stacking (Yilmaz, 2001). In the pre-stacking stage, we removed the random noise and we applied filters and frequency analysis because of compensation for loss of amplitude. We also applied static corrections by refraction (Cox, 1999). A velocity analysis was made using the semblance method (Taner and Koehler, 1969; Neidell and Taner, 1971; Hubral and Krey, 1980). In the stacking stage, velocity analysis was carried out by the constant velocity method (Yilmaz, 2001). In the post-stacking stage, we removed incoherent noise applying the FX deconvolution method (Yilmaz, 2001). Figure 5 shows a strong reflector at about 0.7 s and 2 s in west-east direction (yellow color; top panel) for the 2D view of seismic line 5325. The same figure 5 shows the same line in depth conversion in the bottom panel. It made possible to define the basin basement and some discontinuities associated with faults in the east sector. The geological structures were identified

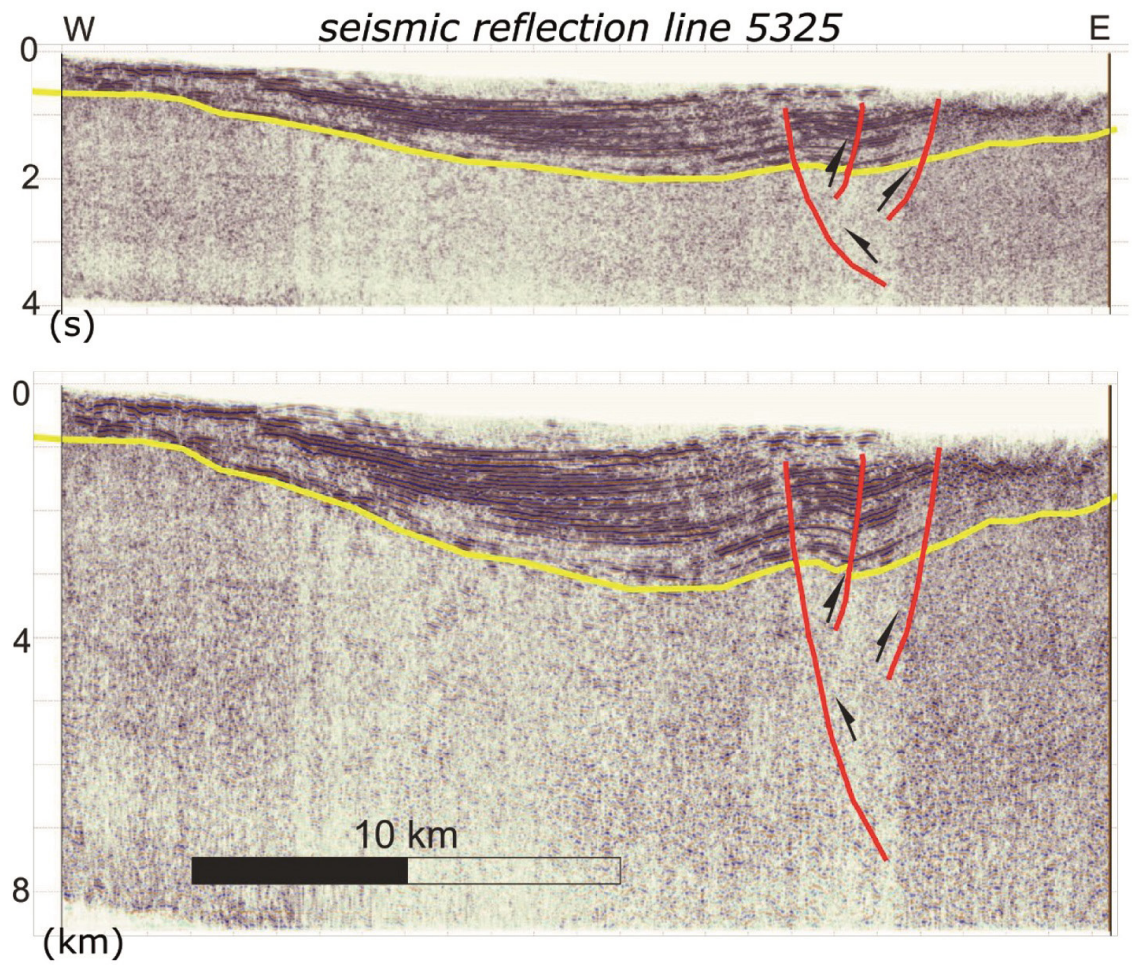

FIG. 5. Seismic reflection Line 5325 (see location in Fig. 3) with vertical axis indicating maximum 4-s two way travel time (TWT) (upper panel) and the corresponding conversion to depth in km (lower panel). A reflector interpreted as the seismic basement is shown in yellow; lateral discontinuities in reflectors in the eastern part of the profile are interpreted as faults (in red), that also affect the basement.

in time and then a depth conversion was made. We note consistency for a similar reflector recognized in all analyzed lines; thus, we interpreted this as the basement of the basin. In addition, several faults were recognized in each seismic line (Fig. 6). After identifying these geological structures in each line, an attempt was made to correlate them with each other and with the structures on the geological map resulting from previous studies (Ré *et al*., 2003; Álvarez-Marrón *et al*., 2006). We used Move software (MVE) and a tool allowing to superimpose surface information such as lithology, geological structures, digital elevation model (DEM) (Fig. 3), among other features.

In order to accomplish a time to depth conversion for the seismic lines a velocity function, representative for the study area, was required. Because of the non-availability of any well data in this region, a direct seismic velocity structure was not an option. Thus, we assumed an average value of v=2,500 m/s for the P wave velocity. This velocity may correspond to the upper (less consolidated) sediments of the basin (Pleistocene and Pliocene) in the following equation. Therefore, for each two way travel time (TWT) a depth can be calculated using $Z(t)=v\,(e^{kt}-1)$ (Marsden, 1992), where Z is the depth in m, k is the rate of change of velocity with depth (we used a value 0.5 Hz),

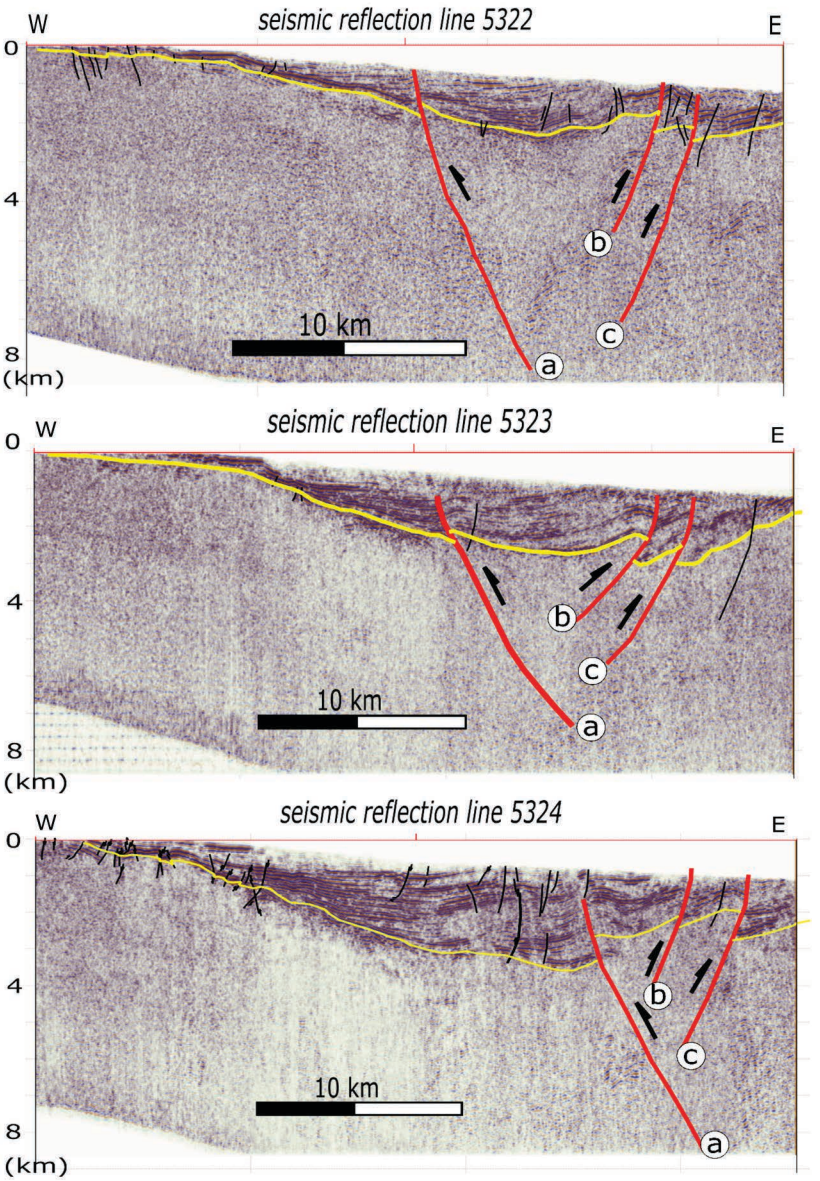

FIG. 6. Processing of seismic reflection lines 5322, 5323 and 5324 show that, from north to south, the basement reaches depths of about 2,100, 2,900 and 3,500 m below the surface, respectively. Major faults (a, b, c) are shown with red color; other minor faults, mainly in the shallower levels, are indicated with black segments. Vertical exaggeration of the sections is 1.5.

and *t* is the time the wave spends to reach the reflector in one single way. Previously detected faults in time (top panel; Fig. 5) were recognized after the conversion from time to depth (bottom panel; Fig. 5). Thus, we completed the analysis for all the lines shown in figure 3. Other examples are shown in figures 6 and 7 for lines 5322, 5323 and 5324, respectively.

5. Results

Assuming that the basement of the basin corresponds to the top of the Carboniferous rocks of the Agua Negra Formation and the velocity function previously described in methodology, the maximum depth to the basement top is of 3,650 m below the surface. This is compatible with results from Beer

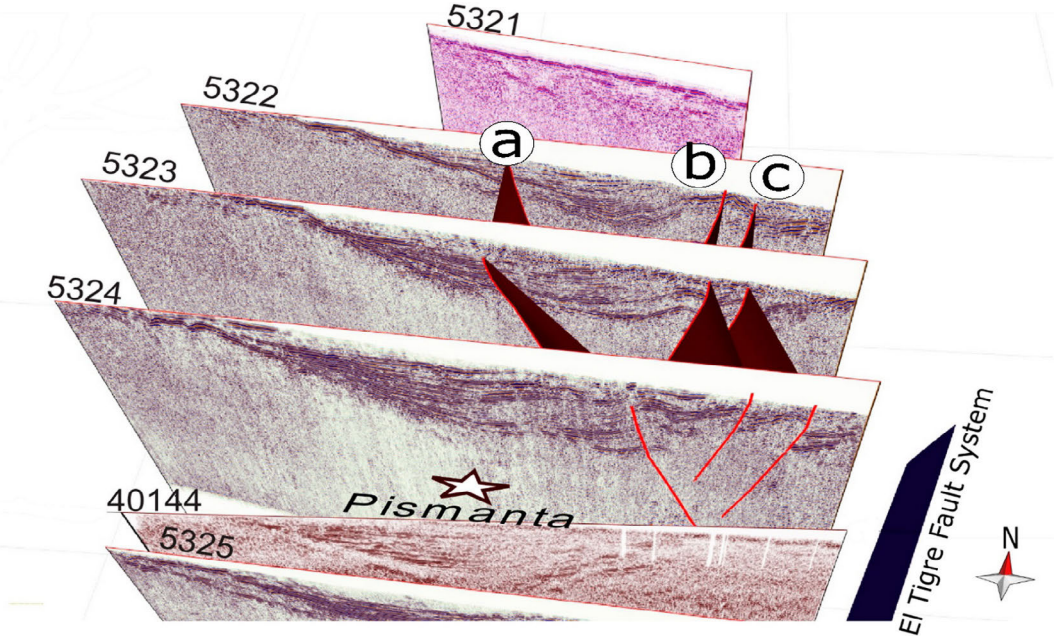

FIG. 7. An integrated view including processed seismic reflection lines 5322, 5323 and 5324 among others in the study area (see Figs. 3 and 6 for details); this information is consistent with a transpressive system involving faults (red lines) elongated in a north-south direction in the eastern part and northwest-trending in the northern part of the study area. The easternmost dark blue structure indicates the approximate location of El Tigre Fault System (Cardó *et al*., 2005).

(1989) and Beer *et al.* (1990), who calculated a maximum depth of the basin of 3,500 m based on interval velocities calculated from seismic reflection data. Figures 8, 9 and 10 show a depocenter (red colors) with three subzones labeled as 1, 2 and 3 for the study region. The location of the maximum depths of the basin correlates with the location of the hot springs at Pismanta area. These three maximum depth areas (of about 20 km radius) are not aligned in a north-south direction. The number 2 area in figure 9 is relatively displaced to the west with respect to areas numbered 1 and 3 probably due to the movement of the inferred faults, which displays a northwest-southeast orientation (labeled as "d" and "e" in Figs. 3 and 9). We have not observed a correlation of these inferred northwest-southeast faults with those shown on surface in the geologic map (Fig. 11). Figure 12 shows faults "d" and "e" along the N-S seismic reflection line 5335, here is inferred that they do not reach the surface. The shape of the basin is not symmetric as can be seen in figures 9 and 10. The basement depth curves are closer together on the eastern border of the basin than on its western side (Fig. 9), where the contours lines maintain a similar horizontal distance from each other. This correlates with the information obtained from seismic lines, which clearly show faults in the eastern sector of the study region, close to the Precordillera, in contrast to the absence of faults towards the western boundary. This is in agreement with the presence of the El Tigre Fault System and the geothermal Pismanta center in its northern part of the basin, above the deepest zones of the Iglesia basin (Fig. 10) according to Gonzalez *et al.* (2020). These authors also provided the first evidence for an extensional control of the basin infill during latest Oligocene (?)-early Miocene.

The analysis of lines 5322, 5323 and 5324 (northern sector of the basin) shows the presence of two faults with depths up to 6 km, which dip approximately 55° westward and another fault located further west with a dip of about 40° eastward and reaching a depth of up to 8 km (Figs. 6, 7 and 8). These structures seem to continue in a horizontal distance of about 40 km and in a north-south direction. We note a correlation with the same exposed structures denoted as "a", "b" and "c" in the geological map of figure 3 as reported by Cardó and Díaz (1999) and Cardó *et al.* (2005).

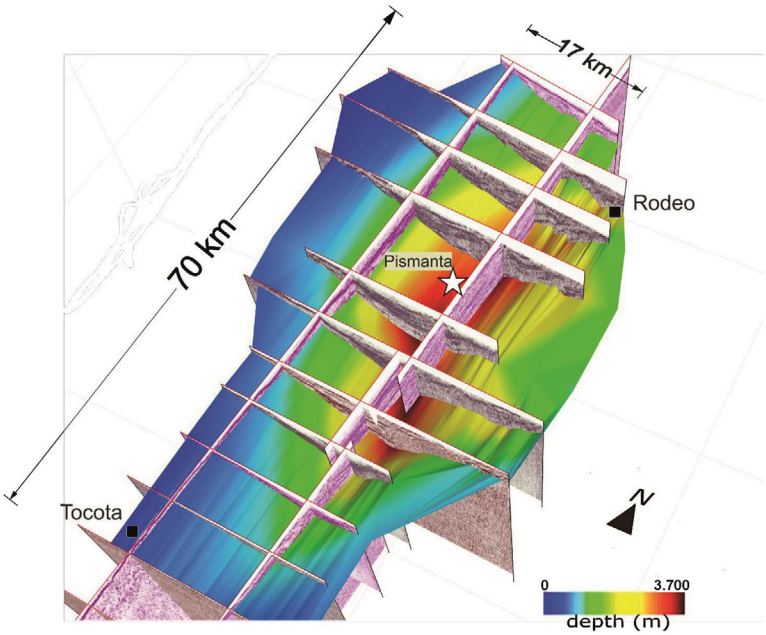

FIG. 8. 3D view of the Iglesia basin shape, based on the processed seismic reflection lines. The Pismanta hot spring location is shown for reference.

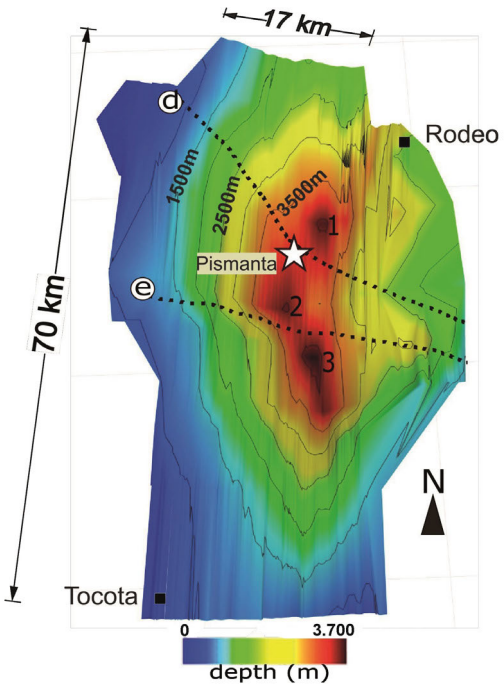

FIG. 9. Map view of the basement topography in the Iglesia basin, after the interpretation shown in figure 6, including contour lines of depths of basement top. Maximum depths of about 3,650 m are localized at three different zones labelled 1, 2 and 3. The inferred faults "e" and "d" are from this study. The average dip angle for the basement in the west margin is 10° (measured in all seismic lines) and 15° for the east.

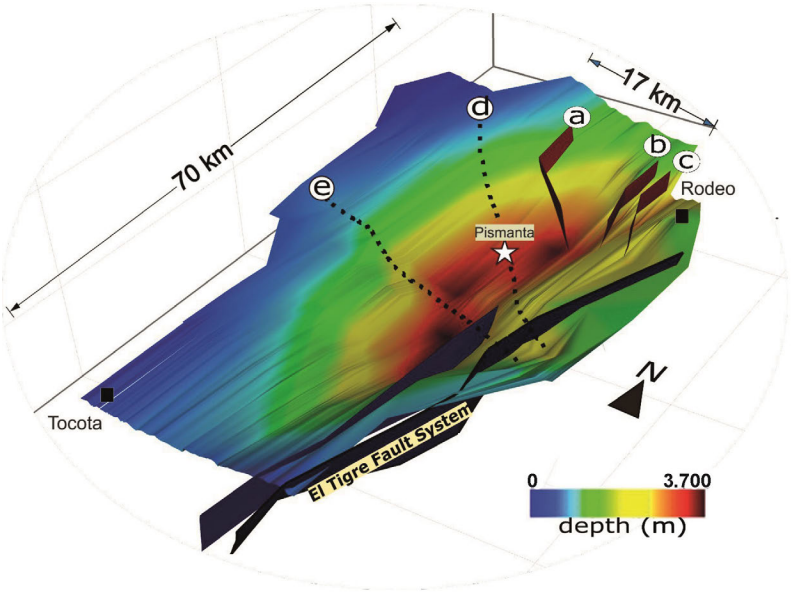

FIG. 10. Geometry of the Iglesia basin with major faults (El Tigre Fault System) and other geophysically interpreted minor faults identified in this work (a, b, c, d and e). Some east-west and northwest-southeast oriented faults are also inferred and might not have an expression on the surface.

Figure 10 shows a geological structure that was identified in the seismic lines and geological mapping, which would correspond to El Tigre Fault System (in dark blue color). These structures may be part of a transpressive fault system (Siame *et al*., 1996, 1997; Fazzito, 2011). Rivas *et al*. (2019) determined local seismic activity between 10 and 30 km depths and analyzed stress field over 33 focal mechanism solutions for the earthquakes (see inset in Fig. 11). Their results show a minimum vertical compressive stress σ_3 and an almost horizontal position for the maximum compressive stress σ_1. Some studies have documented this type of motion along the El Tigre Fault System in the Western Precordillera (*e.g.*, Bastías, 1986; Perucca and Vargas, 2014). The same faults identified in figures 6, 7, 9 and 10 are represented in the map view of figure 11 next to the El Tigre System main fault. This system may be connected to the deepest part of the basement near Pismanta favoring the fluids to reach higher depths and thus higher temperatures, as well as a conduit for transportation to the surface using these high angle faults in the upper 10 km. From its deepest part, the basement goes up steeper toward the east (~20°) while its depth smoothly diminishes toward the west (~15°). We note that several faults recognized in this work in the seismic lines 5322, 5323 and 5324 are affecting both the basin fill and the basement (Figs. 5 and 6).

Figure 10 also shows the correlation of 5322, 5323 and 5324 seismic lines in a three-dimensional perspective. In this view, we have interpolated the presence of the faults that were identified in each 2D seismic line. We used black color in figure 10 for major faults (with depths up to 8 km) and red color for minor faults, showing a north-south continuity of these structures. At deeper levels, there is no other easily identifiable reflector in the basement. The deepest part of the basin is between line 5323 and line 5327. The Pismanta geothermal center is located in the same area. The next step consisted in an integration of all of the previously analyzed and marked seismic reflection lines to generate a 3D model; thus, the location of the basement was interpolated between each pair of seismic lines. We observe three zones of maximum depth in the 3D view, which are summarized in figures 9 and 10.

6. Discussion

Based on the analyzed seismic reflection data covering the Iglesia Valley, we obtained a 3D view indicating an asymmetric basin morphology with three dissected maximum depth zones. In addition,

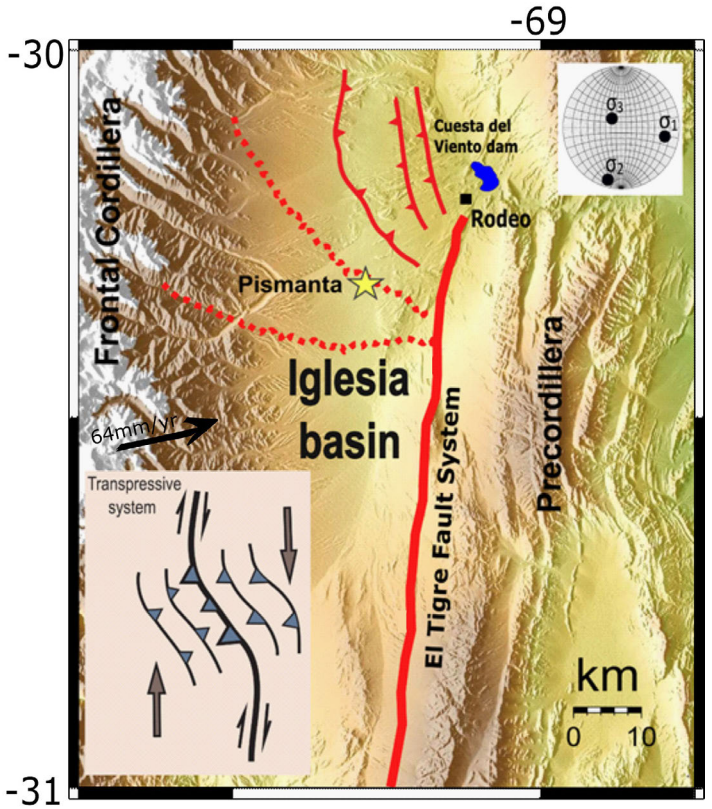

FIG. 11. El Tigre Fault system and other minor faults identified in this work in the Iglesia basin; they show continuity at depth in our 3D model (*e.g.*, Fig. 7). The geothermal Pismanta area (yellow star) and some localities (black squares) are also indicated for reference. The inset in the left bottom corner shows a schematic interpretation of the transpressive system related to El Tigre Fault System based on the geophysical information analyzed in this and another works (Siame *et al.*, 1996; Pérez and Costa, 2006; Fazzito, 2011); indication of right lateral motion for structures has been suggested by neotectonic studies (*e.g.*, Bastías *et al.*, 1984). This agrees with stresses obtained from focal mechanism solutions of crustal seismicity in this region by Rivas *et al.* (2019), with maximum SW-NE compressive horizontal σ1, and minimum compressive vertical σ3.axes (right upper corner).

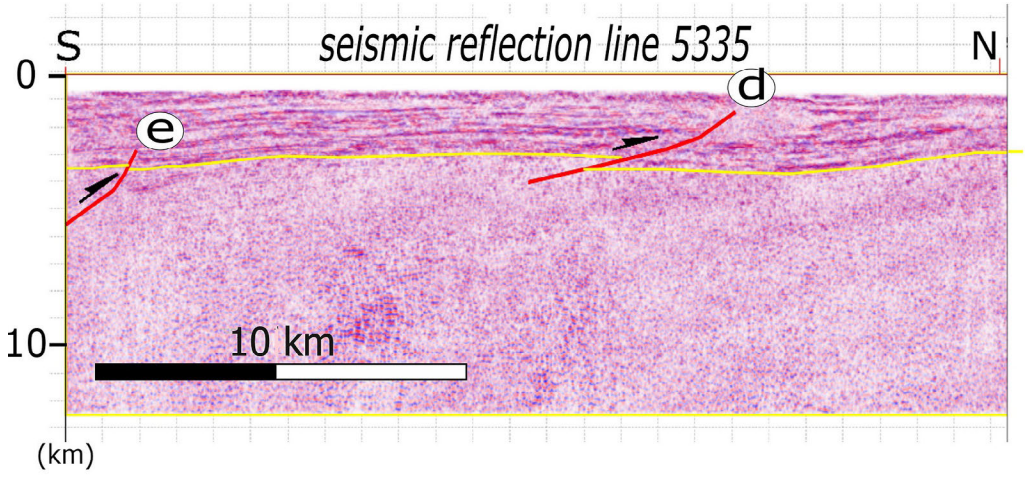

FIG. 12. Cross section along NS seismic reflection line 5335. The inferred e and d faults do not reach to the surface.

we developed a schematic three-dimensional geological diagram located at approximately 30.2° S (Fig. 13). This 3D model integrates surface geological data, regional structural geology from previous studies describing El Tigre Fault system as a flower fault (Álvarez-Marrón *et al*., 2006) and our interpretation of one representative seismic reflection line (5325, Fig. 5). Reflectors showing the top of the basin basement delineate the basin geometry. The interpretation for basement rock units is based on data from neighboring outcrops in the Iglesia basin. Westward, in the Frontal Cordillera, Carboniferous metasedimentary rocks are cropping out, which are intruded by Permo-Triassic rocks (Furque *et al*., 2003). Following an association for the stratigraphy found southward, in the Calingasta basin (Barredo and Ramos, 2010), we could also suggest that Triassic sedimentary rocks might be found beneath the Cenozoic unit in the basin. However, much of the structure beneath the Iglesia basin still remains enigmatic due to seismic reflections lines are only capable of imaging up to 5 km depth and not drilling is available. This last unit would consist mostly of clastic Paleozoic rocks highly deformed, forming large-scale east-verging asymmetric folds, and very low grade of metamorphism (Álvarez-Marrón *et al*., 2006). It is worth to note that this unit crops out eastward being part of the western Precordillera.

Depocenters between two mountain ranges is not a common observation worldwide. The Rocky Mountain Trench (USA) can be considered as a depocenter similar to the andean Iglesia basin, although the tectonic activity is different. Thus, topographic depressions may be controlled by extensional tectonics in the Rocky Mountain Trench (*e.g.*, Van der Velden and Cook, 1996) or by compressional tectonic stresses in the Iglesia basin (Rivas *et al*., 2019). The results observed for the dissected maximum depth areas of the basin, described in the previous item combined with the modeling of the basin and the presence of faults associated with the El Tigre Fault System correlate well with a transpressive system (Siame *et al*., 1996, 1997; Fazzito, 2011) (Fig. 11). The geothermal analysis indicates that El Tigre Fault System plays a role providing conduits for the outflow of heated meteoric waters near Pismanta, above the deepest part of the Iglesia basin and assuming a normal geothermal gradient.

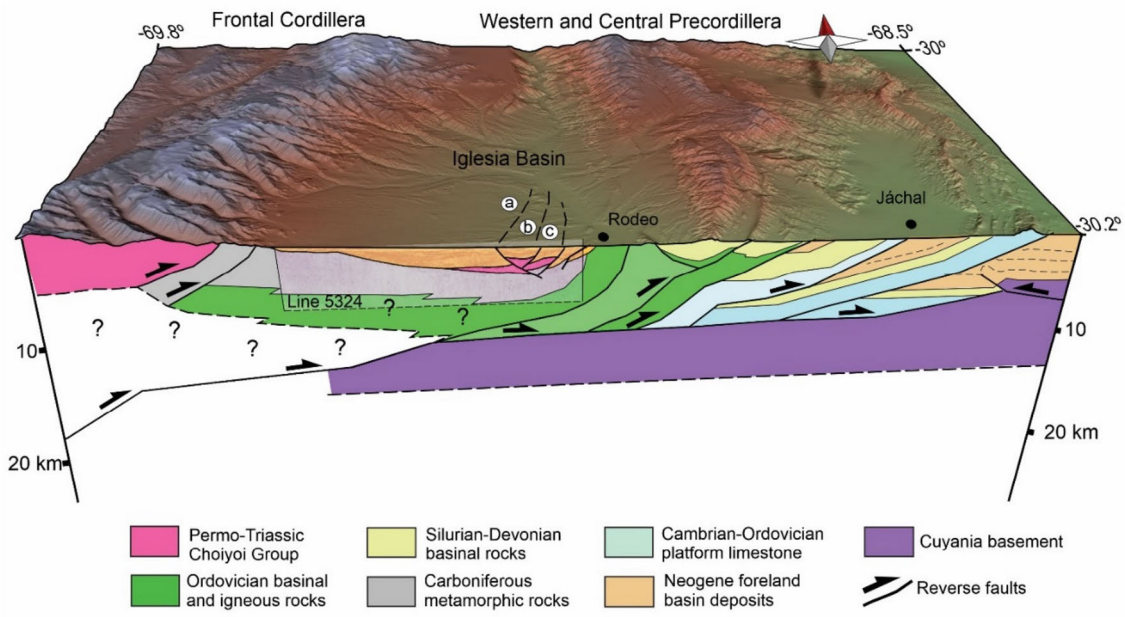

FIG. 13. Schematic structural west-east section at 30.2° S across the Frontal Cordillera and Precordillera. Neotectonic structures at the surface in the Iglesia basin are in dashed lines (see Fig. 3 for references). The lithology and structure beneath the Iglesia basin and Frontal Cordillera are somewhat uncertain due to lack of information (Cardó and Díaz ,1999 and Cardó *et al*., 2005).

7. Conclusions

Processing of 500 km of seismic lines data covering the Iglesia Valley and available geological information has allowed us to obtain a 3D model for the Iglesia basin, located between the Frontal Cordillera and the Western Precordillera of San Juan, Argentina. This helped us to correlate faults recognized at depth (in the seismic lines) with their geological expression at the surface. In three contiguous seismic lines (5322, 5323 and 5324) located between 30°5' S and 30°15' S there are three faults that affect both the Neogene filling of the basin and its Paleozoic basement. The continuity of these structures in a north-south direction is for about 40 km horizontal distance. These minor faults lie in the northern part of the El Tigre Fault and show changes in their dip.

We obtained an asymmetric shape elongated in north-south direction (70x35 km) for the Iglesia basin with three zones of maximum depth of about 3,650 m below the surface. In all seismic lines, geological structures were delimitated showing the presence of a major north-south structure with a high angle dip of about 85° to the west corresponding to the El Tigre Fault System; it exhibits the minor faults with opposed vergences and NW-SE trending in its northern part. Our interpretation corresponds to the presence of a transpressive system associated with the El Tigre Fault, which is consistent with the seismic analysis of the focal mechanism solutions for the earthquakes and the exposed geological information. The water of the hydrothermal system responsible for the hot springs in the Iglesia basin is probably supplied from the west, by meteoric waters infiltrating at the Frontal Cordillera. Thus, the hydrothermal fluids reach relative high temperatures at depth using the faults like fluids paths. The calculated depth of <2 km for the reservoir of Pismanta geothermal system roughly agrees with the depth of basement top. The $^{18}O/^{16}O$ and $^{2}H/^{1}H$ ratios indicate a meteoric origin, in good agreement with fluid migration through the faulting.

The basin exhibits three areas of maximum (3,650 m) depths, beneath Pismanta, which are not aligned in the north-south direction. These three deep zones are relatively horizontally displaced. Thus, we also infer the presence of faults of about 35 km length in a relatively east-west orientation that may be controlling the dissection of the maximum depth zones, although non geological evidence has been already documented.

Acknowledgments

We acknowledge Energía Provincial Sociedad del Estado (EPSE) from the Government of San Juan, Argentina for providing us with geophysical data. Maps were generated using Generic Mapping Tools software (Wessel and Smith, 1998). This work is part of the Research Project PICT2017-676 and PDTS2018-E1092 of Argentina. We thank the Seismotectonics Group of CIGEOBIO-CONICET at the UNSJ for fruitful discussions. We also thank an anonymous reviewer for his valuable comments.

References

Allmendinger, R.W.; Figueroa, D.; Snyder, D.; Beer, J.; Mpodozis, C.; Isacks, B.L. 1990. Foreland shortening and crustal balancing in the Andes at 30° S latitude. Tectonics 9 (4): 789-809.

Álvarez-Marrón, J.; Rodríguez-Fernández, R.; Heredia, N.; Busquets, P.; Colombo, F.; Brown, D. 2006. Neogene structures overprinting Palaeozoic thrust systems in the Andean Precordillera at 30° S latitude. Journal of the Geological Society 163 (6): 949-964.

Ammirati, J.B.; Alvarado, P.; Beck, S. 2015. A lithospheric velocity model for the flat slab region of Argentina from joint inversion of Rayleigh wave phase velocity dispersion and teleseismic receiver functions. Geophysical Journal International 202 (1): 224-241.

Ammirati, J.-B.; Perez Luján, S.; Alvarado, P.; Beck, S.; Rocher, S.; Zandt, G. 2016. High-resolution images above the Pampean flat slab of Argentina (31-32º S) from local receiver functions: Implications on regional tectonics. Earth and Planetary Science Letters 450: 29-39.

Anderson, M.; Alvarado, P.; Zandt, G.; Beck, S. 2007. Geometry and brittle deformation of the subducting Nazca Plate, Central Chile and Argentina. Geophysical Journal International 171 (1): 419-434.

Astini, R.A.; Ramos, V.; Benedetto, J.; Vaccari, N.; Cañas, F.L. 1996. La Precordillera: un terreno exótico a Gondwana. *In* Congreso Geológico Argentino No. 13, Actas 5: 293-324. Buenos Aires.

Barazangi, M.; Isacks, B.L. 1976. Spatial distribution of earthquakes and subduction of the Nazca plate beneath South America. Geology 4 (11): 686-692.

Barcelona, H.; Favetto, A.; Peri, V.G.; Pomposiello, C.; Ostera, H. 2014. Sistema geotermal de despoblados determinado a partir de datos magnetotelúricos, Valle del Cura, San Juan. Revista de la Asociación Geológica Argentina 71 (4): 562-574.

Barcelona, H.; Lelli, M.; Norelli, F.; Peri, G.; Winocur, D. 2019a. Hydrochemical and geological model of the Bañitos-Gollete geothermal system in Valle del Cura, main Andes Cordillera of San Juan, Argentina. Journal of South American Earth Sciences 96: 102378.

Barcelona, H.; Peri, G.; Winocur, D.; Favetto, A. 2019b. Audiomagnetotelluric survey at the Bañitos-Gollete geothermal area, main Andes Cordillera of San Juan, Argentina. Geologica Acta 17: 1-15.

Barredo, S.; Ramos, V.A. 2010. Características tectónicas y tectosedimentarias del hemigraben Rincón Blanco, Cuenca Cuyana: una síntesis. Revista de la Asociación Geológica Argentina 66 (1-2): 133-145.

Bastías, H.; Weidmann, N.; Pérez, M. 1984. Dos zonas de fallamiento Plio-Cuaternario en la Precordillera de San Juan. *In* Congreso Geológico Argentino No. 9, Actas 2: 329-341. San Carlos de Bariloche.

Bastías, H. 1986. Fallamiento Cuaternario en la región sismotectónica de Precordillera: San Juan, Argentina, Tesis de grado (Inédito). Universidad Nacional de San Juan: 147 p.

Beer, J.A. 1989. Magnetic polarity stratigraphy and depositional environments of the Bermejo Basin, and seismic stratigraphy of the Iglesia Basin, Central Andes. Ph.D. Thesis (Unpublished), Cornell University: 1-195.

Beer, J.A.; Allmendinger, R.W.; Figueroa, D.E.; Jordan, T.E. 1990. Seismic stratigraphy of a Neogene piggyback basin, Argentina. American Association of Petroleum Geologists Bulletin 74 (8): 1183-1202.

Benderitter, Y.; Corny, G. 1990. Possible approach to geothermal research and relative cost estimate. Small geothermal resources. UNITAR/UNDP Centre for Small Energy Resources: 61-71 Rome.

Cahill, T.; Isacks, B.L. 1992. Seismicity and shape of the subducted Nazca plate. Journal of Geophysical Research Solid Earth 97 (B12): 17503-17529.

Cardó, R.; Díaz, I. 1999. Hoja Geológica Rodeo (informe preliminar). Servicio Geológico Minero Argentino, Boletín 272. Buenos Aires.

Cardó, R.; Díaz, I.N.; Cegarra, M.I.; Heredia, C.N.; Rodríguez Fernández, R.; Santamaría, G.R.; Fauqué, L.E. 2005. Hoja Geológica 3169-I, Rodeo. Provincia de San Juan. Servicio Geológico Minero Argentino. Boletín 272: 46 p. Buenos Aires.

Costa, C.; Machette, M.; Dart, R.; Bastías, H.; Paredes, J.; Perucca, L.; Tello, G.; Haller, K. 2000. Map and Database of Quaternary Faults and Folds in Argentina. United States Geological Survey, Open-File Report 00-0108: 75 p.

Cox, M. 1999. Static Corrections for Seismic Reflection Surveys. Society of Exploration Geophysicists, Geophysical References Series 9: 531 p. Tulsa.

Cristallini, E.O.; Ramos, V.A. 2000. Thick-skinned and thin-skinned thrusting in the La Ramada fold and thrust belt: crustal evolution of the High Andes of San Juan, Argentina (32° SL). Tectonophysics 317 (3-4): 205-235.

Epstein, S.; Mayeda, T. 1953. Variation of O^{18} content of waters from natural sources. Geochimica et Cosmochimica Acta 4 (5): 213-224.

Fazzito, S.Y. 2011. Estudios geofísicos aplicados a la neotectónica de la falla El Tigre, Precordillera de San Juan. Tesis Doctoral (Inedito), Universidad de Buenos Aires: 291 p.

Fosdick, J.C.; Carrapa, B.; Ortiz, G. 2015. Faulting and erosion in the Argentine Precordillera during changes in subduction regime: Reconciling bedrock cooling and detrital records. Earth and Planetary Science Letters 432: 73-83.

Fournier, R.O. 1983. A method of calculating quartz solubilities in aqueous sodium chloride solutions. Geochimica et Cosmochimica Acta 47 (3): 579-586.

Furque, G.P.; de González, P.; Caballé, M.; Pérez, L.; Cardó, R.; Godeas, M.; Conde, A.; Pucci, J.C. 2003. Hoja Geológica 3169-II, San José de Jáchal. Provincias de San Juan y La Rioja. Instituto de Geología y Recursos Minerales, Servicio Geológico Minero Argentino, Boletín 259: 76 p.

Gonzalez, M.; Clavel, F.; Christiansen, R.; Gianni, G.M.; Lince Klinger, F.; Martinez, P.; Butler, K.; Suriano, J.; Mardonez, D.; Díaz, M. 2020. The Iglesia basin in the southern Central Andes: A record of backarc extension before wedge-top deposition in a foreland basin. Tectonophysics 792: 228590. doi: 10.1016/j.tecto.2020.228590.

Gutscher, M.; Spakman,W.; Bijwaard, H.; Enghdal, R. 2000. Geodynamics of flat subduction: seismicity and tomographic constraints from the Andean Margin. Tectonics 19: 814-833.

Haenel, R.; Rybach, L.; Stegena, L. 1988. Fundamentals of geothermics. *In* Handbook of terrestrial heat-flow density determination (Haenel, R.; Rybach, L.; Stegena, L.; editors). Kluwer Academic Publishers: 9-57. Dordrecht.

Heredia, N.; Fernández, L.R.; Gallastegui, G.; Busquets, P.; Colombo, F. 2002. Geological setting of the Argentine Frontal Cordillera in the flat-slab segment (30°00'-31°30' S latitude). Journal of South American Earth Sciences 15 (1): 79-99.

Hochstein, M.P. 1988. Assessment and modelling of geothermal reservoirs (small utilization schemes). Geothermics 17 (1): 15-49.

Hoke, G.D.; Aranibar, J.N.; Viale, M.; Araneo, D.C.; Llano, C. 2013. Seasonal moisture sources and the isotopic composition of precipitation, rivers, and carbonates across the Andes at 32.5-35.5° S. Geochemistry Geophysics Geosystems 14 (4): 962-978.

Hubral, P.; Krey, T. 1980. Interval Velocities from Seismic Reflection Time Measurements. Society of Exploration Geophysicists: 202 p.

Jordan, T.E.; Allmendinger, R.W.; Damanti, J.F.; Drake, R.E. 1993. Chronology of motion in a complete thrust belt: The Precordillera, 30-31° S, Andes Mountains. Journal of Geology 101: 135-156.

Jordan, T.E.; Schlunegger, F.; Cardozo, N. 2001. Unsteady and spatially variable evolution of the Neogene Andean Bermejo foreland basin, Argentina. Journal of South American Earth Sciences 14: 775-798.

Kay, S.M.; Mpodozis, C.; Ramos, V.A.; Munizaga, F. 1991. Magma source variations for mid-Iate Tertiary magmatic rocks associated with a shallowing subduction zone and a thickening crust in the central Andes (28 to 33° S). *In* Andean magmatism and its tectonic setting (Harmon, R.S.; Rapela, C.W.; editors). Geological Society of America, Special Paper 265: 113-137.

Kay, S.M.; Godoy, E.; Kurtz, A. 2005. Episodic arc migration, crustal thickening, subduction erosion, and magmatism in the south-central Andes. Geological Society of America Bulletin 117 (1-2): 67-88.

Kleiman, L.E.; Japas, M.S. 2009. The Choiyoi volcanic province at 34°S-36° S (San Rafael, Mendoza, Argentina): Implications for the Late Palaeozoic evolution of the southwestern margin of Gondwana. Tectonophysics 473 (3-4): 283-299.

Mackaman-Lofland, C.; Horton, B.K.; Fuentes, F.; Constenius, K.N.; Ketcham, R.A.; Capaldi, T.N.; Stockli, D.F.; Ammirati, J-B.; Alvarado, P.; Orozco, P. 2020. Andean mountain building and foreland basin evolution during thin- and thick-skinned Neogene deformation (32-33° S). Tectonics 39: doi: 10.1029/2019TC005838.

Marsden, D. 1992. V 0-K method of depth conversion. The Leading Edge 11 (8): 53-54.

Muffler, L.J.P. 1979. Assessment of geothermal resources of the United States-1978. United States Geological Survey. Circular 790: 163 p.

Neidell, N.S.; Taner, M.T. 1971. Semblance and other coherency measures for multichannel data. Geophysics 36: 482-497.

Pauwels, H.; Fouillac, C.; Goff, F.; Vuataz, F.D. 1997. The isotopic and chemical composition of CO_2-rich thermal waters in the Mont-Dore region (Massif-Central, France). Applied Geochemistry 12 (4): 411-427.

Peiffer, L.; Bernard-Romero, R.; Mazot, A.; Taran, Y.A.; Guevara, M.; Santoyo, E. 2014. Fluid geochemistry and soil gas fluxes (CO_2-CH_4-H_2S) at a promissory Hot Dry Rock Geothermal System: The Acoculco caldera, Mexico. Journal of Volcanology and Geothermal Research 284: 122-137.

Pérez, I.; Costa, C. 2006. El sistema de fallamiento el Tigre entre el río Jáchal y el cerro Negro de Iglesia (provincia de San Juan). *In* Reunión de Tectónica, No. 13, Actas: p. 80. San Luis.

Pérez, S. 2015. Evolución geotectónica de la faja ofiolítica de Precordillera Occidental. Tesis de Grado (Inédito), Universidad nacional de San Juan, Argentina: 355 p.

Perucca, L.P.; Vargas, N. 2014. Neotectónica de la Provincia de San Juan, centro-oeste de Argentina. Boletín de la Sociedad Geológica Mexicana 66: 291-304.

Pesce, A.H.; Miranda, F. 2003. Catálogo de manifestaciones termales de la República Argentina. Volumen I, Región Noroeste. Provincias de Jujuy, Salta, Catamarca, Tucumán, Santiago del Estero, La Rioja, San Juan. Servicio Geológico Minero Argentino. Anales 36: 165 p. Buenos Aires.

Poma, S.; Ramos, A.; Litvak, V.D.; Quenardelle, S.; Maisonnave, E.B.; Díaz, I. 2017. Southern Central Andes Neogene magmatismo ver the Pampean Flat Slab: implications on cristal and slab melts contribution to magma generationin Precordillera, Western Argentina. Andean Geology 44 (3): 249-274. doi: 10.5027/andgeoV44n3-a02.

Ramos, V.A. 1984. Patagonia: ¿Un continente paleozoico a la deriva? *In* Congreso Geológico Argentino, No. 9, Actas 2: 311-325. San Carlos de Bariloche.

Ramos, V.A. 1995. Sudamérica: un mosaico de continentes y océanos. Ciencia Hoy 6 (32): 24-29.

Ramos, V.A. 1999. Las provincias geológicas del territorio argentino. *In* Geología Argentina (Caminos, R.; editor), Subsecretaria de Minería de la Nación. Servicio Geológico Minero Argentino. Instituto de Geología y Recursos Minerales, Anales 29 (3): 41-96.

Ramos, V.A. 2004. Cuyania, an Exotic Block to Gondwana: Review of a Historical Success and the Present Problems. Gondwana Research 7 (4): 1009-1026.

Ramos, V.A.; Vujovich, G.; Martino, R.; Otamendi, J. 2010. Pampia: a large cratonic block missing in the Rodinia supercontinent. Journal of Geodynamics 50 (3-4): 243-255.

Ré, G.H.; Jordan, T.E.; Kelley, S. 2003. Cronología y paleogeografía del Terciario de la Cuenca Intermontana de Iglesia septentrional, Andes de San Juan, Argentina. Revista de la Asociación Geológica Argentina 58 (1): 31-48.

Rivas, C.; Ortiz, G.; Alvarado, P.; Podesta, M.; Martin, A. 2019. Modern crustal seismicity in the northern Andean Precordillera, Argentina. Tectonophysics 762: 144-158.

Rocher, S.; Vallecillo, G. 2014. Mecanismos eruptivos y procesos depositacionales del Grupo Choiyoi en el área de Las Caletas, Cordillera Frontal de San Juan, Argentina. Andean Geology 41 (3): 589-625. doi: 10.5027/andgeoV41n3-a05.

Ruskin, B.G.; Jordan, T.E. 2007. Climate change across continental sequence boundaries: paleopedology and lithofacies of Iglesia Basin, northwestern Argentina. Journal of Sedimentary Research 77 (9): 661-679.

Siame, L.L.; Sebrier, M.; Bellier, O.; Bourles, D.L.; Castano, J.C.; Araujo, M.; Yiou, F.; Raisbeck, G.M. 1996. Segmentation and horizontal slip-rate estimation of the El Tigre Fault Zone, San Juan Province (Argentina) from SPOT images analysis. Third International Symposium on Andean Geodynamics (ISAG), Proceedings: 239-241. St Malo, France.

Siame, L.L.; Bourles, D.L.; Sebrier, M.; Bellier, O.; Castano, J.C.; Araujo, M.; Perez, M.; Raisbeck, G.M.; Yiou, F. 1997. Cosmogenic dating ranging from 20 to 700 ka of a series of alluvial fan surfaces affected by the El Tigre Fault, Argentina. Geology 25 (11): 975-978.

Sussini, M.; Herrero Ducloux, E.; Brandán, R.; Isnardi, H.; Galmarini, A.; Castillo, M.; Pastore, F.; Corti, H. 1948. Aguas Minerales de la República Argentina, Provincia de San Juan. Ministerio del Interior Comisión Nacional de Climatología y Aguas Minerales (Ley No. 11621), 10: 317 p. Buenos Aires.

Taner, M.T.; Koehler, F. 1969. Velocity spectra-Digital computer derivation and applications of velocity functions. Geophysics 34 (6): 859-881.

Tonani, F.B. 1980. Some remarks on the application of geochemical techniques in geothermal exploration. *In* Advances in European Geothermal Research (Strub, A.S.; Ungemach, P.; editors). Springer: 428-443. Dordrecht.

Vallecillo, G.; Caballero, M.M.; Rocher, S.; Espin, E. 2010. Análisis del Grupo Choiyoi (Permotriásico), Cordillera Frontal de Calingasta, Provincia de San Juan. Revista de la Asociación Geológica Argentina 66 (1): 238-252.

Van der Velden, A.J.; Cook, F.A. 1996. Structure and tectonic development of the southern Rocky Mountain trench. Tectonics 15 (3): 517-544.

Vigny, C.; Rudloff, A.; Ruegg, J.C.; Madariaga, R.; Campos, J.; Alvarez, M. 2009. Upper plate deformation measured by GPS in the Coquimbo Gap, Chile. Physics of the Earth and Planetary Interiors 175 (1-2): 86-95.

von Gosen, W. 1992. Structural evolution of the argentine precordillera: the Río San Juan section. Journal of Structural Geology 14 (6): 643-667.

Wessel, P.; Smith, W.H.F. 1998. New, improved version of Generic Mapping Tools released. Eos, Transactions American Geophysical Union 79 (47): p. 579. doi: 10.1029/98EO00426.

Wetten, C. 1975. Geología del valle de Iglesia, su relación con los yacimientos de diatomita de Lomas del Campanario e importancia económica. Tesis de Grado (Inédito), Universidad Nacional de San Juan, Argentina: 70 p.

Yilmaz, O. 2001. Seismic data analysis: Processing, Inversion and Interpretation of Seismic Data. Investigation in Geophysics No. 10, 1 and 2. Society of Exploration Geophysics: 2027 p. Tulsa.

Manuscript received: June 23, 2020; revised/accepted: September 21, 2021; available online: May 31, 2022.
Editorial handling: Waldo Vivallo